using pseudorandom signature sequences of length $N = 127$, $E_b/N_o \approx 20$dB and $L = 1024$ data bits. Eqn. 2 is evaluated as a function of the normalised offered load $G = gT$ with normalised propagation delay $a = \tau/T$ and channel load threshold K as parameters. A best case value of $\gamma = 2\tau$ is used throughout.

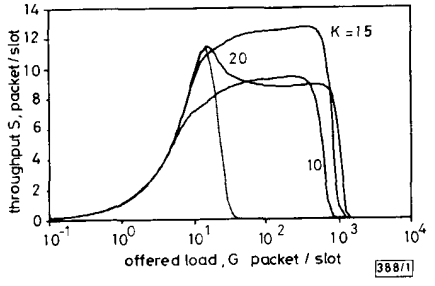

Fig. 1 *Throughput S against offered load G with K as a parameter, a = 0.01*

—— 1P-CSSS/OD
------ slotted CDMA

Fig. 1 shows the throughput S against offered load G for 1P-CSSS/OD with $a = 0.01$ and $K = 10$, 15 and 20 as parameters. The throughput curve for slotted CDMA is plotted for comparison [1,5]. Fig. 1 illustrates that 1P-CSSS/OD achieves a significant throughput improvement over slotted CDMA at large offered loads. The throughput increases with increasing channel load threshold K until the mutual interference of signature sequences produces excessive packet failures. A value of $K = 15$ achieved the optimum throughput performance for the parameters investigated.

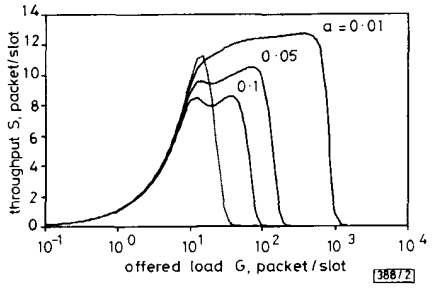

Fig. 2 *Throughput S against offered load G with 'a' as a parameter, K = 15*

—— 1P-CSSS/OD
------ slotted CDMA

Fig. 2 shows the throughput S against offered load G for 1P-CSSS/OD with $K = 15$ and $a = 0.01$, 0.05 and 0.1 as parameters. The throughput curve for slotted CDMA is plotted for comparison. Fig. 2 illustrates that the throughput improvement in 1P-CSSS/OD at high offered loads is due to channel sensing with overload detection and that this strategy is most effective in LANs with a small normalised propagation delay.

Conclusions: The throughput performance of a new 1P-CSSS/OD protocol has been analysed and compared with slotted CDMA for identical channel conditions. The analysis provides a new method for evaluating throughput in SSMA schemes. 1P-CSSS/OD achieves a significant throughput improvement over CDMA at large offered loads. When throughput and offered load are normalised to the channel operating bandwidth (i.e. S/N and G/N), to compare dissimilar multiple access schemes, then at high offered loads 1P-CSSS/OD uses the channel more efficiently than ALOHA whereas CDMA does not. The 1P-CSSS/OD protocol may be applied to packet radio networks, indoor wireless LANs and CDMA cellular mobile networks using an ISMA scheme.

14 June 1993
Electronics Letters Online No: 19931115

T. O'Farrell (*Division of Telecommunications, Asian Institute of Technology, GPO Box 2754, Bangkok 10501, Thailand*)

References

1 O'FARRELL, T., and BEALE, M.: 'Code-division multiple-access (CDMA) techniques in optical fibre LANs.'. Proc. 2nd IEE National Conf. on Telecommun., 1989, (York, United Kingdom), pp. 111–115
2 KLEINROCK, L., and TOBAGI, F.A.: 'Packet switching in radio channels: Part 1-carrier sense multiple access modes and their throughput-delay characteristics', *IEEE Trans.*, 1975, **COM-23**, (12), pp. 1400–1416
3 ROM, R., and SIDI, M.: 'Multiple access protocols: performance and analysis' (Springer-Verlag, 1990)
4 MUSSER, J.M., and DAIGLE, J.N.: 'Throughput analysis of an asynchronous code-division multiple-access (CDMA) system'. Proc. ICC, July 1982, (Philadelphia, PA), pp. 2F.2.1–2F.2.7
5 RAYCHAUDHURI, D.: 'Performance analysis of random access packet switched code division multiple access systems', *IEEE Trans.*, 1981, **COM-29**, (6), pp. 895–901

Wideband 32 × 32 star coupler module with gain

W.Y. Guo, Y.K. Chen, J.Y. Zeng and S. Chi

Indexing terms: Fibre lasers, Optical couplers, Star couplers

A wideband 32 × 32 star coupler module using two fibre amplifiers is presented. Not only can the loss of this module be fully compensated for but also it has better loss uniformity. The power margin increment of 18dB is achieved with this module in a 1.7 Gbit/s system experiment.

Introduction: Large $N \times N$ fibre-optic star couplers play a central role in the architectures of many high-throughput multiple-access WDM networks. However, its inherent $1/N$ splitting loss may limit the ultimate size of the star coupler. Potential use of erbium-doped fibre (EDF) amplifiers to increase the number of users that a fibre-optic star network can support has been investigated by many researchers [1–5]. The number of EDF amplifiers and the choice of their locations in the star network decide the complexity and cost of the network. Among these configurations, the complexity and cost of the proposed scheme in [5] are so far less than those of other configurations. In this Letter, a 32 × 32 star coupler module based on the principle in [5] is constructed and investigated. The power margin increment of 18dB is achieved with this module in a 1.7Gbit/s system experiment.

Description of module: The schematic diagram of the 32 × 32 star coupler module is shown in Fig. 1*a*. It is composed of two 16 × 1 tree couplers, a 2 × 3dB coupler, four optical isolators, two EDF amplifiers in forward pumping scheme and two 1 × 16 tree couplers. Here, these two 16 × 1 tree couplers used are for study, which should be replaced by two 16 × 1 WDM multiplexers in WDM applications. The total passive loss of this module varies somewhat with the channel used and has an average value of ~31dB (14dB before the EDF and 17dB after the EDF) in which the loss of EDF is not included. It is this loss we would like to fully compensate for with two EDF amplifiers. The home-made EDF had a core size of 4.2μm and an NA of 0.23. There are two 0.98μm pump laser diodes in this module; each pump laser with 50 mW output power is efficiently coupled into the 12.3m EDF by a 0.98/1.55μm WDM coupler. The dimension of this 32 × 32 star coupler module as shown in Fig. 1*b* is 32 × 20 × 40cm, which can be reduced to a more compact size with some care of arrangement. In the experiment, a pigtailed 1550nm DFB laser transmitter is directly modulated by a 1.7Gbit/s [$2^{31} - 1$] NRZ pseudorandom data stream and the receiver used is composed of a 0.4nm optical bandpass filter and an avalanche photodiode, which has –35.7 dBm sensitivity for 10^{-9} bit error rate (BER) at 1.7Gbit/s.

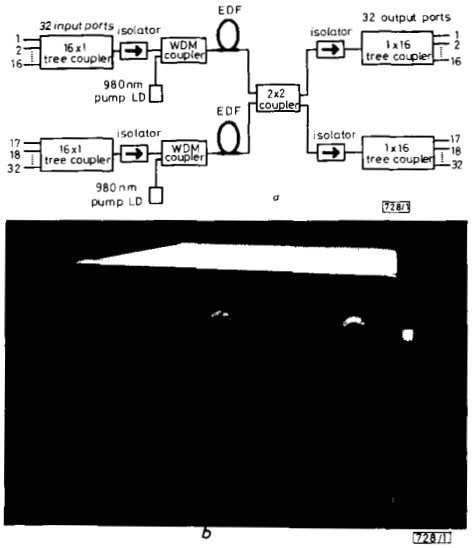

Fig. 1 *32 × 32 star coupler module*

a Schematic diagram
b Photograph of module

Performance of module: Fig. 2 shows the spectral loss characteristics of this module for a single input channel with four different input signal powers. The small-signal system net gain at 1530nm is slightly higher than that at 1550nm. Note that the variations of system loss are less than 2.0dB for P_i equal to −3dBm in the spectral range from 1528nm to 1565nm. The system loss of this module can be fully compensated for when the input signal power is less than −10dBm. The measured system saturated output signal power of this module is −4.6dBm. This output signal power is approximately equal to the total saturated output power expected for multichannel applications. Further improvement of the saturation power may be achieved by using a more efficient EDF or increasing the pump power. Furthermore, the uniformity property of system insertion loss of this module is less than 1.3dB.

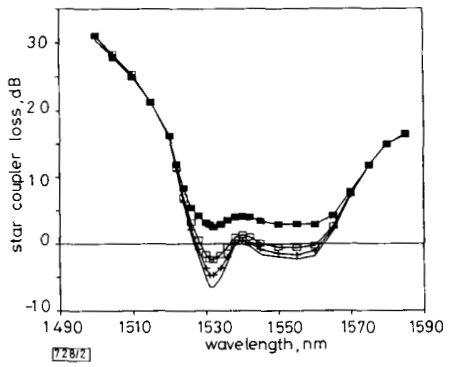

Fig. 2 *Spectral loss characteristics of module for various input signal powers*

P_i = −3dBm
P_i = −10dBm
P_i = −25dBm
P_i = −20dBm

The system sensitivity of this module for 10^{-9} BER at 1.7Gbit/s is −35.0dBm at 1550nm, and there is ~0.7dB power penalty due to the amplified spontaneous emission (ASE) noise resulting from these two activating EDF amplifiers with the transmitter input power of −15dBm. Fig. 3 shows the power penalty and power margin increment of this module for a single channel at 1550nm. The lower input power level into this module the higher power

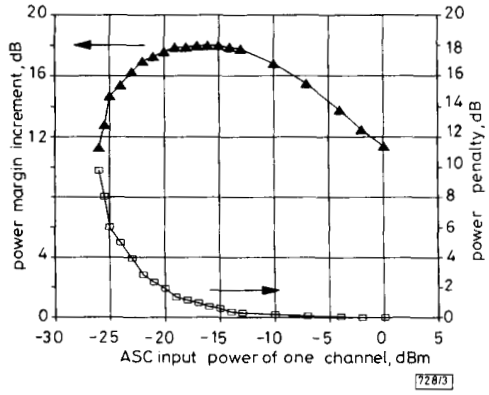

Fig. 3 *Power penalty and power margin increment of module*

penalty, which is due to the large nondepleted ASE noise with respect to smaller input signal power. The power margin increment is defined as the power margin enhancement, at 10^{-9} BER, of this amplified module over a passive 32 × 32 star coupler with ~17dB insertion loss. The increment is contributed by the compensated module loss and power penalty of the transmitting signal. There is an increment of about 18dB for input powers in the range −19 to −13dBm; however, this power margin decreases for input power levels beyond this range. Fig. 4 shows the spectral characteristics of power penalty and power margin increment of this module for a 1550nm input signal at channel 1 with a P_i of −15dBm and the input channel 2 (namely crosschannel) at various wavelengths with an input power of 15 times that of channel 1. The power margin increment is larger than 12dB and the power penalty is less than 0.6dB in the spectral range 1520–1570nm.

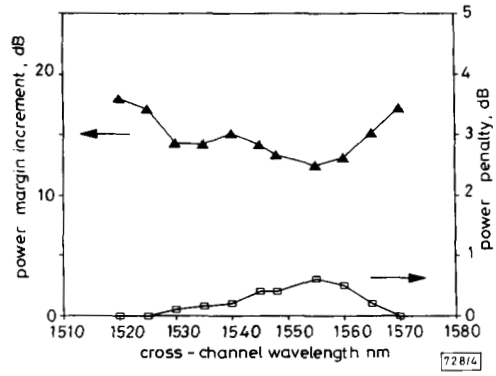

Fig. 4 *Spectral characteristics of power penalty and power margin increment*

Conclusions: We have presented a 32 × 32 star coupler module using two EDF amplifiers. The pump power use efficiency of this module (i.e. 32 port/100mW) is, to our knowledge, the highest yet reported. Not only can the loss of this module be fully compensated over a wide spectral range, but also has better loss uniformity, low power penalty and high power margin increment. The demonstration of this proposed technique makes feasible the construction of a large star coupler for wideband star networks.

Acknowledgments: The authors wish to thank the entire optical Fiber and Optoelectronic Technology team, and Y. K. Tu for his support.

12 July 1993
Electronics Letters Online No: 19931131

W. Y. Guo, Y. K. Chen and J. Y. Zeng (*Telecommunication Laboratories, Ministry of Transportation and Communications, Taiwan, Republic of China*)

S. Chi (*Institute of Electro-Optical Engineering and Center for Telecommunications Research, National Chaio-Tung University, Hsinchu, Taiwan, Republic of China*)

References

1 WILLNER, A.E., SALEH, A.A., PRESBY, H.M., DIGIOVANNI, D.J., and EDWARDS, C.A.: 'Star couplers with gain using multiple erbium-doped fibres pumped with a single laser', *IEEE Photonics Technol. Lett.*, 1991, **3**, (3), pp. 250–252
2 PRESBY, H.M., and GILES, C.R.: 'Amplified integrated star coupler with zero loss', *IEEE Photonics Technol. Lett.*, 1991, **3**, (8), pp. 724–726
3 IRSHID, M., and KAVEHRAD, M.: 'Star couplers with gain using fiber amplifiers', *IEEE Photonics Technol. Lett.*, 1992, **4**, (1), pp. 58–60
4 CHEN, Y.K., CHI, S., and LIAW, J.W.: 'Hybrid transmissive optical star couplers with gain using fiber amplifiers', *IEEE Photonics Technol. Lett.*, 1993, **5**, (2), pp. 230–232
5 CHEN, Y.K., and CHI, S.: 'WDM/FDM star coupler with gain using fibre amplifiers', *Electron. Lett.*, 1993, **29**, (9), pp. 731–732

Accurate physical fusion taper shape model for waveguide analyses

S. Lochmann, J.-M. Labs and A.B. Sharma

Indexing terms: Optical fibre fabrication, Optical couplers

A model for predicting the accurate shape of fusion tapers depending on fabrication parameters has been developed and applied to the sensitive tapering of DC fibres resulting in short lowloss tapers.

Introduction: Thermically tapered fibre-optic devices such as couplers, wavelength division de/multiplexers and micro-ring resonators require an accurate understanding of the relationship between technological and device parameters. No exhaustive theoretical model is available which considers technological parameters and relates them to the characteristics of fused optical components. For example, fusion couplers have been analysed by using either the mean fibre diameter or a linear or exponential approximation for the taper geometry [1, 2]. Empirical studies of the pulling process of taper couplers mentioned in [3], which related gas flow parameters to diameter variations approximated by a second order polynomial, provided a more accurate model but still lacked generality.

This Letter describes an accurate method for analytically determining the shape of thermically tapered fibres. Thus the model establishes the relationship between the technological parameters of elongation, pulling speed and temperature distribution and the resulting taper geometry. The diameter variation is then used for optimising taper geometries as one typical application example. Compared to matched-cladding (MC) fibres which are usually used for fused taper devices, depressed-cladding (DC) fibres need very smooth taper structures [4] that would normally result in impractical taper lengths of the order of half a metre or more. However, using the model presented in this Letter it has been possible to predict and fabricate shaped tapers from DC fibres which are comparable to MC fibres in terms of taper length and losses.

Theory: The process of pulling glass fibres in the range of their softening temperature (i.e. log η = 7.6) can be described by

$$\frac{d\left(\frac{l}{l_0}\right)}{dt} = K \cdot \frac{F}{A} \tag{1}$$

where l/l_0 is the relative elongation, F is the pulling force, A is the fibre cross-section and $K = (3\eta)^{-1}$ [5] is a constant related to viscosity η.

By quantising to m volume elements V_i of any small size which is shown in Fig. 1, a description of the diameter variation at any fibre position can be developed where

$$V_i = \frac{V}{m} = \frac{\pi}{4} \cdot d_i^2 \cdot l_i \tag{2}$$

If the fibre is fixed on one side then the overall pulling speed V_T results from the sum of the individual elongation speeds. For a taper process that makes use of two moving jigs the overall pulling speed would result from a vectorial summation of the jig velocity, thus

$$v_T = \sum_{i=1}^{m} v_i \tag{3}$$

Comparing this approach with the well known serial connection of spring elements in mechanical engineering we can assume a constant drawing force at any volume element. Therefore eqn. 4 holds.

$$v_i = \frac{\Delta l_i}{\Delta t} \simeq F \cdot \frac{l_i}{3\eta_i A_i} \tag{4}$$

Normalising gives a coefficient ranging from 0 to 1 which yields the individual elongation speed v_i after multiplication with the overall pulling speed v_T described by

$$v_i = \frac{\frac{l_i}{3\eta_i A_i}}{\sum_{i=1}^{m} \frac{l_i}{3\eta_i A_i}} \cdot v_T \tag{5}$$

Thus the elongation of any volume element l_i during a time interval Δt can be calculated which yields the new diameter, respectively, because of the volume constancy.

$$d_i = \sqrt{\frac{4V_i}{\pi(l_i + \Delta l_i)}} \tag{6}$$

Because the viscosity of silica glass is related very closely (±3K) to the applied temperature due to the Vogel-Fulcher-Thamman equation [6] the diameter variation of the tapered fibre can be determined in terms of the elongation, the pulling speed and the temperature distribution.

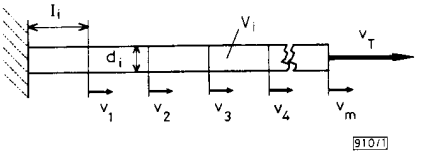

Fig. 1 *Schematic diagram fibre tapering model*

The validity of the model follows for the following conditions:
(i) The volume of the fibre is constant (i.e. thermal expansion can be neglected).
(ii) The impact of flame pressure and gravity can be ignored because they have to be excluded anyhow by means of relatively low tapering temperatures (<2000°C) in order to avoid losses due to micro-bending.
(iii) The influence of the surface tension can be neglected because of the mentioned low tapering temperature (the forces caused by surface tension on a taper volume element are typically two magnitudes below those due to the pulling process, thus no improvement has been achieved).

Calculating the local diameter and hence the local core radius variation da/dz yields the essential parameter for evaluating possible losses due to launching of higher order modes. Thus an immediate comparison with the allowed phase differences of the HE_{11} and typically the HE_{12} mode or the HE_{11coax} mode of the coaxial waveguide in the case of DC fibres can be carried out [4] because

$$\frac{|da|}{dz} < \frac{a \cdot |\beta_{HE_{11}} - \beta_{HE_{12}/HE_{11coax}}|}{2\pi} \tag{7}$$

Experiment: A specific burner with 13 individually controlled nozzles provided the capability of a wide variety of temperature profiles over a 20mm range. Based on a temperature distribution with a 1930°C dip at the edges of the burner and a smooth 1820°C central dip, a constant pulling speed of 20μm/s and an elongation of